Sensitivity of the C and O production on the 3α rate

H. Schlattl (hs@astro.livjm.ac.uk)
Astrophysics Research Institute, Liverpool John Moores University, Twelve Quays House, Egerton Wharf, Birkenhead CH41 1LD, UK

A. Heger (1@2sn.org)
Department of Astronomy and Astrophysics, University of Chicago, 5640 South Ellis Avenue, Chicago, IL 60637, USA, and
Theoretical Astrophysics Division, T-6, MS B227, Los Alamos National Laboratory, Los Alamos, NM 87545, USA

H. Oberhummer (ohu@kph.tuwien.ac.at)
Atominstitut of the Austrian Universities, Technische Universität Wien, Wiedner Hauptstraße 8–10, A-1040 Wien, Austria

T. Rauscher (tommy@quasar.physik.unibas.ch)
Departement für Physik und Astronomie, Universität Basel, CH-4056 Basel, Switzerland

A. Csótó (csoto@matrix.elte.hu)
Department of Atomic Physics, Eötvös University, Pázmány Péter sétány 1/A, H-1117 Budapest, Hungary

Abstract. We investigate the dependence of the carbon and oxygen production in stars on the 3α rate by varying the energy of the 0_2^+-state of ^{12}C and determine the resulting yields for a selection of low-mass, intermediate-mass, and massive stars. The yields are obtained using modern stellar evolution codes that follow the entire evolution of massive stars, including the supernova explosion, and consider in detail the 3$^{\rm rd}$ dredge-up process during the thermally pulsating asymptotic giant branch of low-mass and intermediate-mass stars. Our results show that the C and O production in massive stars depends strongly on the initial mass, and that it is crucial to follow the entire evolution. A rather strong C production during the He-shell flashes compared to quiescent He burning leads to a lower sensitivity of the C and O production in low-mass and intermediate-mass stars on the 3α-rate than predicted in our previous work. In particular, the C production of intermediate-mass stars seems to have a maximum close to the actual value of the 0_2^+ energy level of ^{12}C.

Keywords: stars: abundances – stars: late-type – stars: evolution – stars: interiors

1. Introduction

The large binding energy of the α-particle as compared to its neighbouring nuclei with $A < 12$ leads to a unique situation: In order to create elements heavier than $A > 7$ by fusion of lighter isotopes, high temperatures and densities should be needed. This already puzzled astrophysics in the middle of the 20$^{\rm th}$ century, as under such conditions

newly created carbon would almost immediately be fused further to form heavier elements. As a result, only tiny amounts of carbon would be produced, which is in contradiction to the abundances observed in the universe.

Hoyle et al. (1953) concluded that a then unknown excited state in the ^{12}C nucleus must exist with an energy close to the 3α-threshold (see also Hoyle, 1954). This resonance would strongly increase the probability that the short-living ^{8}Be nucleus can capture a further α-particle. Indeed, the 0_2^+-state of ^{12}C had been found experimentally later (Cook et al., 1957), with an energy of $372 \pm 4\,\mathrm{keV}$ above the ground state of three α-particles, close to the value predicted by Hoyle et al. (1953). The modern value of the resonance energy E_R^0 is $379.47 \pm 0.15\,\mathrm{keV}$ (Firestone et al., 1996).

Since the reaction rate of the 3α-process is basically determined by only one resonance, the C-production crucially depends on the energy level of this 0_2^+-state. If the resonance energy were higher, essentially all ^{12}C would be processed further to ^{16}O due to the hotter conditions at the ignition of the 3α reactions. Reducing the energy level would lead to the consumption of all α-particles by the 3α-reaction, and thus no ^{16}O could be created.

Livio et al. (1989) found that the carbon production in intermediate-mass and massive stars is inhibited, if the energy level is increased by about 250 keV, while a 60 keV increase still yields considerable quantities of ^{12}C. Based on nuclear models, we claimed (Oberhummer et al., 2000, Paper I) that a change by about 0.5 % in the strength of the nuclear force, or of 4 % in the Coulomb force, corresponding to a shift in the 0_2^+ energy level of about 130 keV, suffices to inhibit either C or O production in stars.

Examining H I 21-cm and molecular QSO absorption lines, Murphy et al. (2001) recently found indications for a variable fine-structure constant (α_F). According to their analysis $\Delta\alpha_\mathrm{F}/\alpha_\mathrm{F} = (-0.72 \pm 0.18) \times 10^{-5}$ for a redshift range $0.5 < z < 3.5$. This would lead to a small alteration in the Coulomb force and thus to modified atomic and nuclear physics during this period. The consequent changes in equation of state, opacity or nuclear reaction rates, however, are too small to alter the evolution of stars considerably, as pointed out by Fiorentini and Ricci (2002).

Although the resonance energy of ^{12}C would hardly be shifted by the measured difference in α_F, there are various circumstances where higher changes in E_R^0 are conceivable: First, in Grand Unified Theories (GUT) the varying fine structure constant would imply that the coupling constants of the other fundamental forces are also variable. For example, the relative change in the QCD scale parameter, Λ, would be about a factor 30 to 60 larger than the rel-

ative change in $\alpha_{\rm F}$ (Langacker et al., 2002, Calmet and Fritsch, 2002, Dent and Fairbairn, 2003)[1]. Depending on the model of the nucleon force the observed value of $\Delta\alpha_{\rm F}/\alpha_{\rm F}$ would then result in a change of up to a few keV in the resonance energy (Oberhummer et al., 2003). Second, it is not clear what kind of time-dependence $\alpha_{\rm F}$ is showing, and, in particular, what value $\alpha_{\rm F}$ had during $z > 3.5$.

Accounting solely for the uncertainties in GUT and nucleon models, changes in the C and O yields of a few 10% are not inconceivable, when considering the results of Livio et al. (1989) and Paper I. In none of these two works, however, was the *full* evolution of the stars followed. In particular, the exact dredge-up process in low- and intermediate-mass stars was not considered in detail, and later evolutionary stages in massive stars, including explosive nucleosynthesis in the supernova and remnant formation (fallback of supernova ejecta), were neglected. In the latter case some O could be produced in neon burning independent of the 3α-rate.

In this work, we followed the evolution of 1.3 and $5\,M_\odot$ stars through their whole asymptotic giant-branch (AGB) evolution using five different values of the resonance energy. The evolution of 15 and $25\,M_\odot$ stars was followed until onset of core collapse and through the supernova explosion using the standard value of the 0_2^+ energy level and cases where it was raised or lowered by 100 keV.

We would like to emphasize that the changes in the energy of the carbon resonance we considered are not based on the assumption that the experimental resonance energy is not well known. Rather, we assumed hypothetical changes in the resonance energy, which may be caused by, for example, a varying fine structure constant. Our aim is to contribute to the ongoing discussions mentioned above by showing what changes in the carbon and oxygen production can realistically be expected over the considered range of energy shift. The comparison with results from galacto-chemical evolution models enables to give first rough limits on what variations in the resonance energy are allowed. Additionally, our detailed models provide better estimates for the "fine-tuning" of carbon and oxygen production in stars required to create considerable amounts of these two key elements necessary to enable carbon-based life. In particular, we show that the fine-tuning arguments of Paper I have been considerably weakened.

The changes in the resonance energy considered in this work can already be caused by weak modifications in the underlying nuclear physics, like, e.g., the QCD scale parameter (see, e.g., Oberhummer

[1] An exception is the model of Chacko et al. (2002), which does not necessarily lead to a change in Λ.

et al., 2003). Such changes are too small to alter considerably the rates of other reactions, in particular of ^{12}C(α,γ)^{16}O, which competes with the 3α process during stellar He burning (Oberhummer et al., 2001). For instance, shifting the subthreshold resonances, which determine the ^{12}C(α,γ)^{16}O rate, by the same amount as the 0_2^+ energy level would result in a two orders of magnitude smaller change for the ^{12}C(α,γ)^{16}O than for the 3α rate at astrophysically relevant temperatures. Furthermore, the non-resonant contribution in the 3α reaction rate (Langanke et al., 1986) always remains negligible over the considered range of energy shift.

2. Stellar input physics

2.1. Massive stars

Models of 15 $M_\odot$ and 25 $M_\odot$ Population I stars were calculated using the current version of the implicit stellar evolution code KEPLER (Weaver et al., 1978, Woosley and Weaver, 1995, Heger et al., 2000, Rauscher et al., 2002). A stellar model typically employs of the order of a thousand Lagrangian mass zones that adopt to the structure as needed to resolve gradients of temperature, density, composition, etc. For these calculations we used essentially the same opacity tables as described below for the intermediate mass stars. Only for temperatures above 10^8 K were the opacities of Woosley and Weaver (1995) and Weaver et al. (1978) used. Mass loss by stellar winds was implemented using the rate given by Nieuwenhuijzen and de Jager (1990). Convection (mixing-length theory) and semiconvection were treated as described in Weaver et al. (1978) and Weaver and Woosley (1993) using a time-dependent diffusion approach (see also Woosley et al., 2002, for a recent summary).

We used the approximative 19-isotope network described by Weaver et al. (1978) but include updated nuclear reaction rates (Rauscher et al., 2002). The network includes light isotopes and all α-nuclei up to ^{56}Ni, plus Fe isotopes. This is sufficient to trace the change in the C and O abundances through all burning stages. Only in the late stages of stellar evolution are nuclear statistical equilibrium (NSE) and quasi-NSE networks used to follow the weak interactions in silicon burning and in the iron core in more detail. The networks are directly coupled to the hydrodynamical computation and provide the nuclear energy generation rate in a self-consistent and energy-conservative way.

Note that the He-burning results (and thus the yields of the later burning stages) also depend on the ^{12}C(α,γ)^{16}O rate. It is a well-known and long-standing problem in nuclear astrophysics to determine

this rate and its temperature dependence to sufficient accuracy at the relevant temperatures. Despite many efforts, the current experimental accuracy (Buchmann, 1996, Kunz et al., 2001, Kunz et al., 2002) leaves enough room for considerable variation in the rate and the resulting evolution. The effects of an altered $^{12}C(\alpha,\gamma)^{16}O$ rate on the evolution of massive stars were studied in the same approach in Weaver and Woosley (1993), Heger et al. (2002), and Woosley et al. (2003). Nevertheless, it must be emphasized that the effects of a variation of the 3α rate as investigated here go far beyond the change seen in those models. Therefore, we kept the $^{12}C(\alpha,\gamma)^{16}O$ rate fixed here and used 1.2 times the rate of Buchmann (1996), yielding a cross section of about $S(300\,\mathrm{keV}) = 170\,\mathrm{keV}$ barn as recommended by Weaver and Woosley (1993). This treatment is also consistent with recent measurements by Kunz et al. (2001) and Kunz et al. (2002).

2.2. Low- and intermediate-mass stars

The low-mass and intermediate-mass stars were computed using the Garching stellar evolution code (Weiss and Schlattl, 2000), which is able to follow the evolution through the He flash of low-mass stars (Schlattl et al., 2001, Cassisi et al., 2003b) and through the thermally pulsating asymptotic giant branch (TP AGB, Wagenhuber and Weiss, 1994) until the white-dwarf cooling track. Up-to-date input physics was used in the model computations, including the OPAL opacities (Iglesias and Rogers, 1996), completed in the low-temperature regime by the tables of Alexander and Fergusson (1994). For the equation of state the analytic description by A. Irwin was employed (see, e.g., Cassisi et al., 2003a, for a brief description), which is similar to the OPAL equation of state (Rogers et al., 1996) for solar conditions (see, e.g., Schlattl, 2002), but is valid in a much larger metallicity, temperature, and density range. The temperature gradients in convective regions, defined by the Schwarzschild-criterion, were obtained from the mixing-length theory (Böhm-Vitense, 1958) using the parameter $\alpha = 1.59$. For the outer boundary condition of the star an Eddington grey atmosphere was chosen.

All the major nuclear reactions relevant to determine the final abundances of C and O during the TP AGB evolution are included in the code. The main H-burning reaction rates were taken from Adelberger et al. (1998) and for He-burning rates of Caughlan et al. (1985) were used. In the relevant temperature range ($0.15 < T/(10^8\,\mathrm{K}) < 0.3$), the resulting $^{12}C(\alpha,\gamma)^{16}O$-rate is about 20–40 % higher than the most recent value of Kunz et al. (2002).

During the standard evolution H- and He-burning are well separated within the star, and therefore two different nuclear networks were applied. In convective regions that contain nuclear reactions the chemical evolution was followed by subsequent mixing and burning steps. However, when H was engulfed in He-burning regions, both networks were treated automatically in a common scheme, which also incorporates the mixing in convective regions (Schlattl, 1999). For this purpose, a time-dependent mixing approach was used similar to the KEPLER code, i.e., the instantaneous mixing within convective regions usually assumed is substituted by a fast diffusive process (Langer et al., 1985).

3. Evolutionary stellar models

3.1. Massive stars

Using the KEPLER code (§2.1) we followed the evolution of six models from main-sequence hydrogen burning to the onset of core collapse and through the supernova explosion. For each mass, 15 and 25 $M_\odot$, a complete stellar evolution calculation was performed with the standard 3α rate and two calculations with rates modified by varying the 0_2^+ energy level of ^{12}C by $\Delta E_\mathrm{R} = E_\mathrm{R} - E_\mathrm{R}^0 = \pm 100\,\mathrm{keV}$.

3.1.1. *The standard evolution*

A detailed description of the evolution of massive stars can be found, e.g., in Limongi et al. (2000) or Woosley et al. (2002). Here we just provide a brief description of the burning phases.

In the middle panels of Figs. 1 and 2 the evolution of 15 and 25 $M_\odot$ stars using the standard value of the 3α rate are shown in a Kippenhahn diagram. The first two convective central burning phases are hydrogen and helium burning. A few 10,000 years after the stars have finished core He burning, carbon burning ignites, producing mainly ^{20}Ne by ^{12}C(^{12}C,α)^{20}Ne, where the α-particles are captured dominantly by ^{16}O to form further ^{20}Ne. Depending on the carbon abundance remaining after central helium burning and on the central entropy, which decreases with increasing core size, central carbon burning starts convectively or radiatively. The carbon abundance also determines how extended the shell burning phases are and how long they last. The location of the last carbon shell persists until core collapse, setting the size of the carbon-free core. Larger cores usually form bigger iron cores, determining, in turn, whether a neutron star or black hole results.

Only a few thousand years after ignition of C burning, the core temperature reaches values at which ^{20}Ne photo-disintegrates to ^{16}O+α

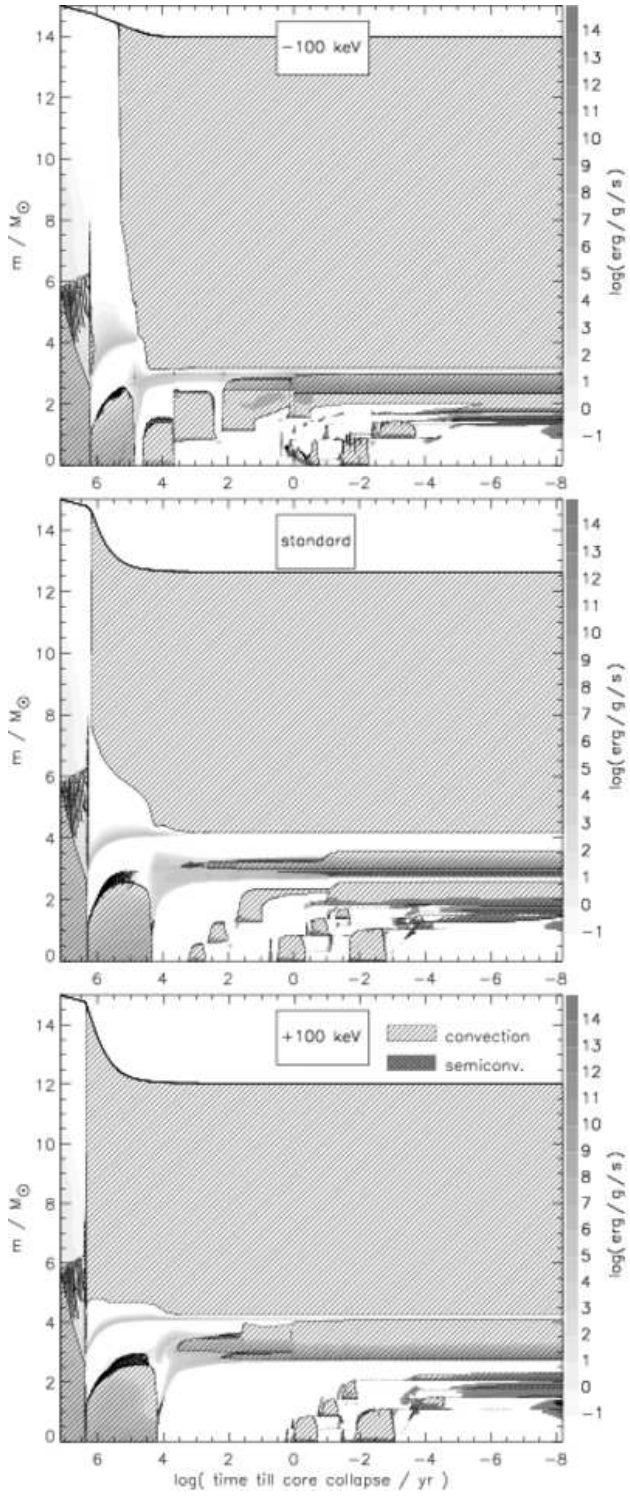

Figure 1. Kippenhahn diagrams of $15\,M_\odot$ stars are shown for the three cases: $\Delta E_{\rm R} = -100$ (top), 0 (middle), and +100 (bottom). Convection zones are indicated by diagonal hatching and a solid line is drawn around them (the cascade of convective zones above the convective core during hydrogen burning thus appears black). Semiconvection is marked by diagonal cross hatching. Specific nuclear energy generation minus neutrino losses, where positive, is indicated by grey shading. The uppermost line indicates the total mass of the star, decreasing due to stellar winds.

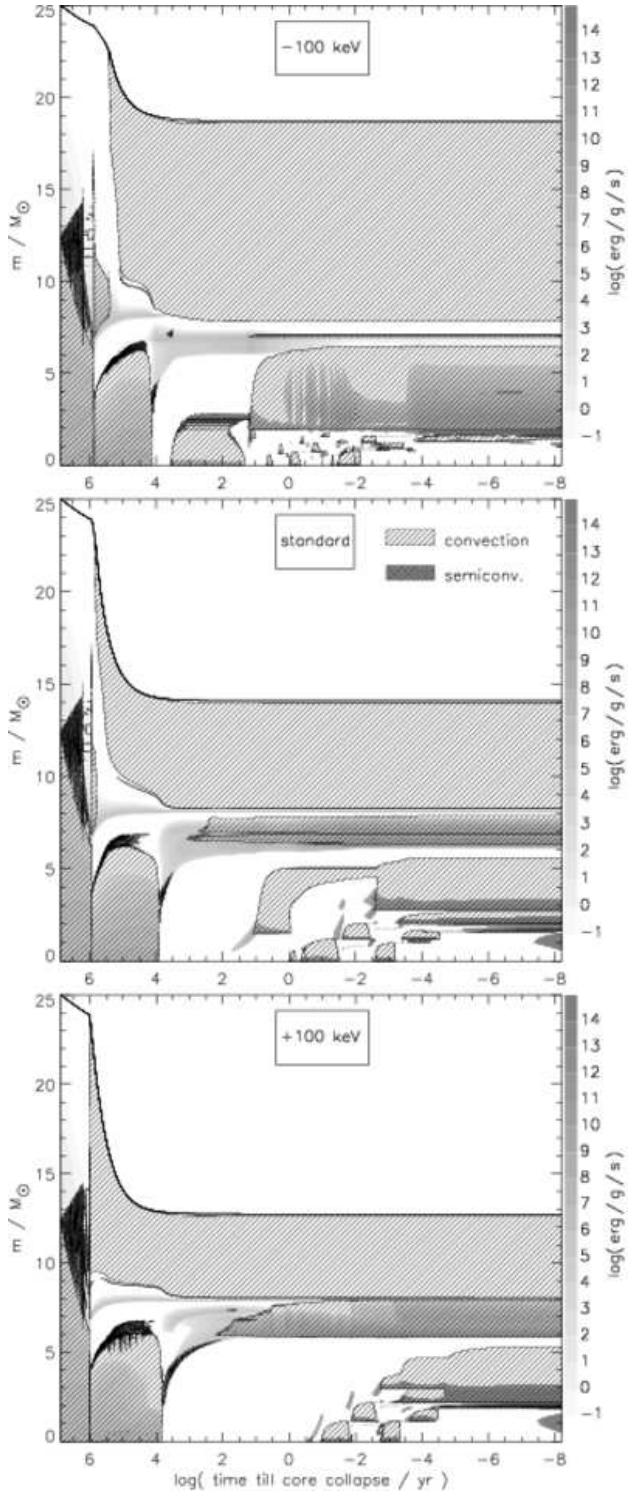

Figure 2. Same as Fig. 1, but for $25\,M_\odot$ stars.

(neon burning). The liberated α particles are captured producing α-nuclei from ^{24}Mg to ^{32}S. The next burning phase is oxygen burning, fusing two ^{16}O nuclei and producing nuclei like ^{28}Si, ^{32}S, and ^{34}S (by additional captures). Central O burning lasts only a few months to a few years. This is followed by a few hours or days of silicon burning, producing iron group elements, and is the last burning phase before core collapse. The collapse occurs when the iron core has grown sufficiently large. An explosion ensues, to current knowledge likely driven by neutrinos from the hot neutron star (Woosley et al., 2002, Janka et al., 2002). A shock front runs through the stars and induces explosive nucleosynthesis. The reaction paths relevant for explosive carbon and oxygen burning are similar to those in the hydrostatic burning phases, but occur at higher temperature and on a much shorter time scale.

We emphasize that the apparent small change in the ejected oxygen mass (Table I) is not a trivial result: carbon and neon are burnt to oxygen, while oxygen is being burnt to magnesium, silicon and heavier elements.

The supernova explosion was simulated by a piston located at the big rise in entropy usually co-located with the base of the oxygen burning shell, the most likely location for a successful launch of the supernova shock (H.-T. Janka, 2002, private communication). Here, we employed an entropy of $S = 4\,k_{\rm B}$/baryon to place the base of the piston. The piston was first moved inward to 500 km, accelerating at a constant fraction of the local gravitational acceleration (25 %, fitting collapse models by H.-T. Janka and M. Rampp, 2002, private communication). Subsequently it was moved outward to 10,000 km where it reached zero velocity and was stopped. The piston was decelerated at a constant fraction of the local gravitational acceleration. Acceleration and initial velocity after bounce were adjusted to match a kinetic energy of the ejecta of 1.2×10^{51} erg (more details will be provided in Heger, A. & Woosley, S. E., in preparation). How much mass was ejected or fell back onto the remnant was then determined by following the hydrodynamical evolution of the supernova and its nucleosynthesis.

The resulting masses of C and O in the stellar ejecta are summarized in Table I. In order to obtain metallicity-independent yields, we subtracted the amount of C and O in the envelope, and we also excluded the inner part of the core that later becomes part of the remnant. That is, the sums given in Table I only comprise the layers with mass coordinates between that of the remnant and the helium core mass given in Table III. The central evolution of the star and the obtained C and O yields in the supernova ejecta are fairly independent of the

Table I. Total mass of C and O in the helium core ejected by the supernova for the 15 and 25 $M_\odot$ stars. We only include the masses in the ejecta but disregard the hydrogen envelope (see text) as well as mass in regions that later become part of the remnant. In each of the two sections, the upper rows give carbon and oxygen masses after core helium depletion, the second rows the masses after core carbon burning when a central temperature of 1.2×10^9 K is reached, the third rows that at onset of core collapse and the bottom rows the yields after the supernova explosions.

	15 $M_\odot$			25 $M_\odot$		
$\frac{\Delta E_R}{\mathrm{keV}}$	−100	0	+100	−100	0	+100
$M_{\mathrm{He}}(\mathrm{C})$	1.05	0.32	0.00	3.69	1.03	0.00
$M_{\mathrm{C}}(\mathrm{C})$	0.38	0.21	0.01	3.11	0.72	0.01
$M_{\mathrm{col}}(\mathrm{C})$	0.36	0.13	0.02	2.65	0.34	0.02
$M_{\mathrm{SN}}(\mathrm{C})$	0.36	0.13	0.02	2.57	0.34	0.02
$M_{\mathrm{He}}(\mathrm{O})$	0.04	0.87	0.46	1.20	3.60	2.11
$M_{\mathrm{C}}(\mathrm{O})$	0.02	0.85	0.46	0.95	3.50	2.04
$M_{\mathrm{col}}(\mathrm{O})$	0.05	0.86	0.48	0.79	3.27	1.84
$M_{\mathrm{SN}}(\mathrm{O})$	0.06	0.71	0.33	0.81	3.09	1.64

initial composition, while this not true for some rarer isotopes like the *s*-process.

Although the CNO cycle does slightly affect the carbon and oxygen yields of massive stars by changing the envelope content in the 1$^{\mathrm{st}}$ and/or 2$^{\mathrm{nd}}$ dredge-up, these yields would strongly depend on the initial abundance ratio of CNO isotopes made by earlier generations of massive and intermediate-mass stars. Since we are interested in the effect of varying the α reaction rate on the yields of certain types of stars, without considering the full chemical history of their initial material, we remove the contribution of initial abundances from our analysis. Note that in the standard case the amount of C and O in the envelope is negligible compared to their abundances in the interior, but it would influence the results in the case where $\Delta E_{\mathrm{R}} = -100\,\mathrm{keV}$. For this case in particular, the reduction of carbon in the envelope by the CNO cycle is significant compared with the total carbon made.

In contrast to carbon, oxygen is produced in *two* phases of hydrostatic stellar nucleosynthesis: in the helium and in the neon burning. Both C and O are destroyed, in part, in the core by later hydrostatic burning phases. The oxygen abundance is additionally affected by explosive nucleosynthesis while carbon is not changed much by the supernova shock. Therefore, we provide the carbon and oxygen yields at four stages in Table I: after central helium and carbon depletion,

Table II. Central mass fractions (%) of key elements after core helium depletion for the 15 and 25 $M_\odot$ stars.

	15 $M_\odot$			25 $M_\odot$		
$\frac{\Delta E_R}{keV}$	−100	0	+100	−100	0	+100
C	93.03	21.47	<0.01	73.20	19.11	<0.01
O	4.68	76.16	49.76	24.49	78.17	45.41
Ne	1.96	2.03	14.25	1.97	2.33	15.08
Mg	0.07	0.08	35.65	0.08	0.12	39.17
Si	0.08	0.08	0.15	0.08	0.08	0.15
S	0.04	0.04	0.04	0.04	0.04	0.04

at core collapse, and after the supernova explosion. For central helium depletion we additionally give the central mass fractions of key elements in Table II.

3.1.2. *Models with* $\Delta E_R = -100\,keV$

When reducing ΔE_R, the ignition of He fusion took place at lower temperature, where $^{12}C(\alpha,\gamma)^{16}O$ is less efficient. Thus, less oxygen was produced during this phase as shown in detail in Paper I. Due to a limited nuclear network, in Paper I the evolution of the massive stars was followed only until a core temperature of 10^9 K, roughly corresponding to the end of core C burning.

Therefore, several effects could not be accounted for. Firstly, the higher amount of C created in models with $\Delta E_R = -100\,keV$ might lead, during C burning, to an enhanced Ne production, and thus the O yield of neon burning might be bigger than in the standard case. Secondly, different composition, temperature, and density profiles of the star after core C burning influence the subsequent evolution, leading to different final sizes of the Ne/Mg/O core (abbreviated as 'Ne/O core' in Table III) and of the Si core. That is, the amount of carbon and oxygen burnt in the star until it reached core collapse was not determined. Thirdly, oxygen is also destroyed during the explosive burning of the supernova. Finally, in case the iron core is too big to make a powerful explosion, a significant part of the oxygen-rich layers may fall back onto the remnant and form a black hole. Here we assumed that all stars resulted in successful explosions with 1.2×10^{51} erg kinetic energy of the ejecta and we obtained no fallback of oxygen or carbon.

To demonstrate the second point, in addition to Figs. 1 and 2, we show in Fig. 3 the evolution of central density and temperature. Due to the lower resonance energy, helium burning started at a lower tem-

Table III. Properties of 15 and 25 $M_\odot$ stars at onset of core collapse. Here $M_{\rm preSN}$ is the final stellar mass. All masses are in units of $M_\odot$. The last column gives the remnant mass (baryonic mass) including fall back after the supernova explosion assuming a kinetic energy of the ejecta of 1.2×10^{51} erg.

$\frac{\Delta E_{\rm R}}{\rm keV}$	15 $M_\odot$			25 $M_\odot$		
	−100	0	+100	−100	0	+100
$M_{\rm preSN}$	14.0	12.6	12.0	18.7	14.1	12.7
He core	3.10†	4.10	4.11	7.83†	8.09	7.91
C/O core	2.35	2.77	2.77	6.48	6.26	5.87
Ne/O core	1.72	1.86	2.77	1.84	2.73	5.87
Si core	1.42	1.70	2.05	1.66	2.10	2.85
Fe core	1.42	1.54	1.58	1.64	1.69	1.88
remnant	1.63	1.71	2.05	1.78	2.05	2.19

† Helium core mass reduced due to dredge-up.

perature, as shown in the lower left corner of the figures. After helium burning, the larger amount of carbon caused more extended and longer-lasting carbon shell burning. This was followed by well-expressed neon burning shells in the 25 $M_\odot$ star inside a small carbon-free core, or even by off-centre neon ignition (due to high degeneracy) in the 15 $M_\odot$ star. Indeed, the core of the 25 $M_\odot$ star with lowered resonance energy seems to have some similarity with the 15 $M_\odot$ standard case.

As a likely consequence of helium burning at higher entropy (higher temperature and lower density), the star also encountered a dredge-up of the outer layers of the helium core, because the entropy step at the edge of the core was decreased. Note that the modified models spent a significant time of their helium burning phase as blue stars with radiative envelopes.

The final C and O yields of these stars are provided in Table I. In the 25 $M_\odot$ star with the lowered resonance energy, oxygen was still efficiently destroyed in the hydrostatic burning phases after core helium depletion. In the 15 $M_\odot$ star, however, oxygen was produced. For both masses a small amount of oxygen was made in the supernova explosion. In the 25 $M_\odot$ star the carbon shell was so deep inside the star that 0.08 $M_\odot$ of C was destroyed. In this star, 0.023 $M_\odot$ of O was made here in explosive carbon and neon burning, while in the underlying Ne/Mg/O layer 0.001 $M_\odot$ oxygen was destroyed and only nickel and silicon were made. In the 15 $M_\odot$ star 0.015 $M_\odot$ of oxygen was destroyed in Ne/Mg/O layer and at the base of the C shell in explosive

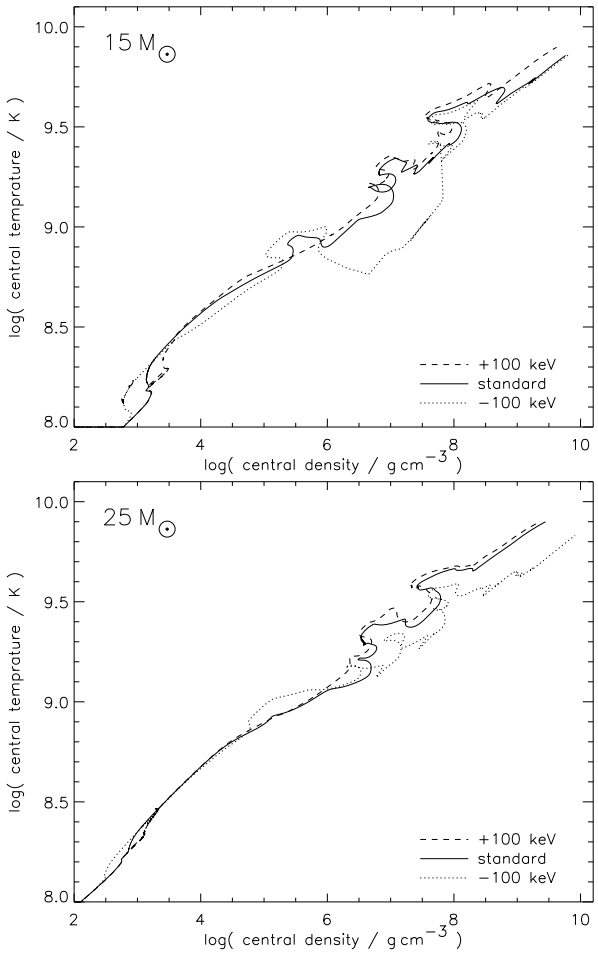

Figure 3. Upper Panel: Evolution of central temperature and central density in $15\,M_\odot$ stars after hydrogen depletion is shown for the three cases: $\Delta E_{\rm R} = -100$ (dotted line), 0 (solid), and +100 (dashed). Generally, massive stars evolve to higher central densities and temperatures, but degeneracy and central and shell burning stages cause several 'wiggles' along the way. *Lower Panel:* same but for $25\,M_\odot$ stars.

nucleosynthesis (and a trace at the base of the He shell), but $0.027\,M_\odot$ oxygen was made.

3.1.3. *Models with* $\Delta E_{\rm R} = +100\,$keV

When the resonance energy was increased, helium burning ignited and proceeded at higher temperature (Fig. 3). At these high temperatures the $^{12}{\rm C}(\alpha,\gamma)^{16}{\rm O}$ reaction effectively destroyed any carbon made. The core was more compact and more luminous, resulting in a more extended convective red supergiant envelope, developing very

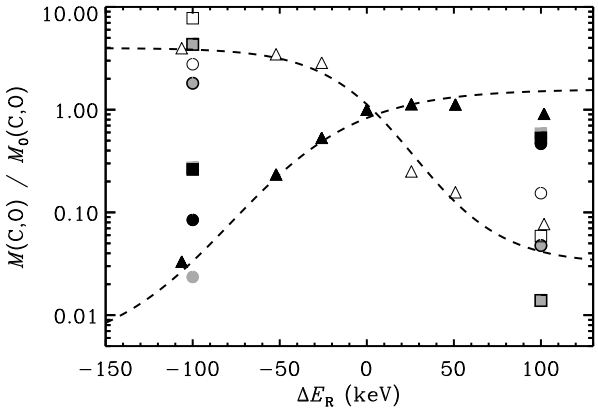

Figure 4. Dependence of the overall amount of C and O produced in massive stars on $E_{\rm R}$. The SN yields of Table I are shown as black ○'s ($15\,M_\odot$) and □'s ($25\,M_\odot$), where the open and filled symbols denote C and O, respectively. The yields after core C exhaustion are marked by grey symbols (solid: O, framed: C). For comparison, the results obtained in Paper I are indicated by open and solid △'s, and the dashed line helps to guide the eye.

rapidly after core hydrogen depletion and exerting higher wind mass loss (Figs. 1 and 2). At the end of helium burning, essentially no carbon was left (Table II). Significant amounts of heavier elements, neon and magnesium, were made already in central helium burning. Consequently there was no carbon shell burning that would have affected the contraction of the helium-free core. However, neon burning was a well developed convective phase — but now due to neon made in helium burning rather than carbon burning. This was followed by extended central and shell oxygen burning phases, and resulted in a big iron core of high entropy.

In the $15\,M_\odot$ star the production and destruction of oxygen were about balanced — oxygen burning competed with converting the neon made in helium burning into oxygen, slightly favouring oxygen production. Conversely, in the $25\,M_\odot$ star the large extent of the oxygen burning shells reduced the oxygen yield. In both cases a significant amount of oxygen was destroyed in the supernova explosion, but as most of the carbon contained in the helium core was made in the helium-burning shell, the carbon yields was not affected.

3.1.4. *Summary*

In Fig. 4 we show the variation of the C and O production in the 15 and $25\,M_\odot$ stars as a function of the resonance energy. Overall, the behaviour is similar to the results of Paper I, where a $20\,M_\odot$

star was followed until core C depletion using the Garching stellar evolution code. In the SN yields we find less underproduction of C ($\Delta E_{\rm R} = 100\,{\rm keV}$) or O ($\Delta E_{\rm R} = -100\,{\rm keV}$) than predicted in Paper I. In particular, the O yields in the $25\,M_\odot$ star for $\Delta E_{\rm R} = 100\,{\rm keV}$ are only diminished by about a factor of 4, while Paper I predicted a reduction that is higher by almost one order of magnitude. In the few models we have computed, for both $\Delta E_{\rm R} = -100$ and $+100\,{\rm keV}$ more C and O tended to be retained or created after core C burning than in the standard case. The post C-burning evolution and the resulting carbon and oxygen yields depend on the extent of the different burning zones and their interaction in the course of late stellar evolution. This can vary strongly as a function of initial mass and thus a trend more along the line of Paper I may result if averaging over a larger set of initial masses is done (using an initial mass function).

Several reasons may be responsible for obtaining different results than in Paper I. Firstly, we used a different stellar evolution code (KEPLER) than in Paper I (Garching stellar evolution code) that uses a different $^{12}{\rm C}(\alpha,\gamma)^{16}{\rm O}$ reaction rate, a key ingredient for the resulting C/O ratio. KEPLER implements a different treatment of convective boundaries (overshooting) and semiconvection (operating in regions that are stable against convection according to the Ledoux but not the Schwarzschild criterion). The latter process has an important role in massive stars. Secondly, our new calculations followed the entire evolution of the star through the supernova explosion, and therefore we can determine how much mass falls back onto the remnant. The yields provided in the present paper (Table I and Fig. 4) self-consistently exclude this inner region of the star, unlike in Paper I where this information was not available. For comparison, the overall yields after core C burning obtained using the KEPLER code are given here as well. The relative change of the yields when modifying $E_{\rm R}$ was, however, not significantly different from the results shown in Fig. 4. Therefore we conclude that most of the discrepancies between Paper I and the present work are indeed caused by the different physics applied.

Our results show that the suppression of C and O in the appropriate case is smaller and depends on the initial mass. It is essential to follow the complete evolution of the star at least until the pre-collapse phase to obtain reliable results for each stellar mass. The destruction of oxygen by explosive oxygen burning and the production of oxygen by explosive neon burning during the supernova explosion may give non-negligible contributions. In particular explosive nucleosynthesis may always produce some oxygen, even in the case of rather low $\Delta E_{\rm R}$ values. Comparing the yields of the 15 and $25\,M_\odot$ stars before and after the SN explosion (Table I), the minimum amount of O produced could be

as high as $\sim 0.01\,M_\odot$. This would lead to a maximal suppression of the O production for $\Delta E_{\rm R} < 0$ to about a few 0.1%.

3.2. Intermediate-mass stars

We computed sequences of $5\,M_\odot$ stars from the ZAMS to the end of the AGB for 5 different values of the 0_2^+ resonance energy in ^{12}C using the Garching stellar evolution code (§2.2). The initial composition was chosen to be scaled solar with [Fe/H] $= -2.3$. Similar to massive stars, the influence of the initial metallicity on the final C and O production is small for intermediate-mass stars.

The sequences could not be followed through the final pulse due to a considerable reduction of the gas pressure with a concomitant super-Eddington luminosity. Under this condition the star cannot be treated in quasi-static equilibrium, and thus the models fail to converge. However, the envelope will be removed from the nucleus by a radiation-driven wind, and the remnant will become a white dwarf (Wood and Faulkner, 1986, Faulkner, 1970, Finzi and Wolf, 1971). Thus, by combining the abundances in the wind and in the stellar envelope, a good measure of the total amount of C and O ejected into the inter-stellar medium (ISM) by the stars under scrutiny is obtained.

Mass loss was implemented according to Reimers (1975) with an efficiency parameter $\eta = 0.8$. To model the strong winds on the tip of the AGB a description as used, e.g., by Marigo et al. (1996) was applied, accounting for the mass loss during Mira and super-wind phase (see also Vassiliadis and Wood, 1993).

3.2.1. *The standard case*

In Fig. 5 we show the evolution in the H-R diagram of a model with standard 3α-rate for about 50 pulses along the TP AGB. With each pulse the star slowly becomes cooler due to the gradual enrichment of the surface, mainly by carbon, due to the 3$^{\rm rd}$ dredge-up. We outline this mechanism in Fig. 6: during the quiescent He-burning phase between 2 pulses, the He shell becomes gradually thinner and thus thermally unstable (see, e.g., Kippenhahn and Weigert, 1990). The increasing rate of energy release within this shell creates a convection zone between the H and He shell (inter-shell convection zone: ISCZ) which is enriched by He-burning products. The He shell and the overlying layers start to expand and to cool (Fig. 6b,c), reducing the H-burning efficiency until it eventually ceases (Fig. 6d).

After the He-shell flash, the convective envelope deepens, penetrating into regions previously occupied by the ISCZ. In this way, newly

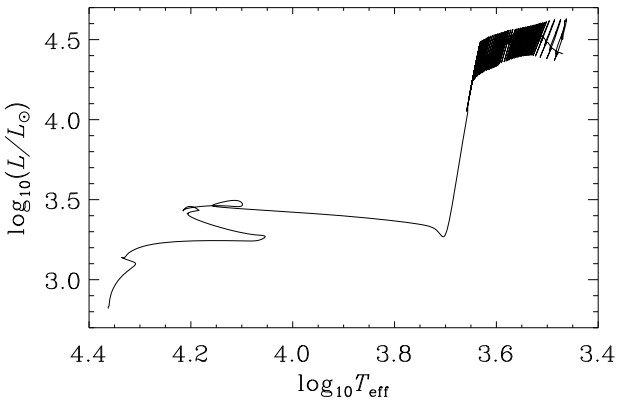

Figure 5. Evolution of a $5\,M_\odot$ star in the H-R diagram.

created ^{12}C is mixed to the surface ("3$^{\rm rd}$ dredge up"). In the subsequent evolution the outer layers contract, and both H- and He-burning shells are restored. When the He-burning shell becomes unstable again, the next thermal pulse ensues.

Since the region of the ISCZ is subsequently covered by He and H burning reactions, a variety of nuclear processes take place. This includes some reactions that produce neutrons. In particular in more massive stars these reactions are thought to be sufficiently abundant to create elements beyond Fe by the so-called "*s*-process". In the present paper, however, we are only interested in the total C and O production of the star, which poses less demands on the nuclear reaction network.

The C and O abundances in the ISCZ crucially depend on the relative strengths of the 3α and ^{12}C+α reactions during the He-shell flash. To illustrate their efficiency inside the star, we have plotted in Fig. 7

$$f_\sigma^{\rm CO} = \frac{\sigma_n^{3\alpha}}{\sigma_n^{{\rm C}\alpha} + \sigma_n^{3\alpha}}, \tag{1}$$

where

$$\begin{aligned} \sigma_n^{3\alpha} &= \frac{\dot{n}_{\rm C}}{n_{\rm He}^3} = \frac{1}{6}\frac{\varrho}{m_u}\langle\sigma v\rangle_{3\alpha} \quad \text{and} \\ \sigma_n^{{\rm C}\alpha} &= \frac{\dot{n}_{\rm O}}{n_{\rm C} n_{\rm He}} = \frac{\varrho}{m_u}\langle\sigma v\rangle_{^{12}{\rm C}+\alpha} \end{aligned} \tag{2}$$

with n, ϱ, m_u and $\langle\sigma v\rangle$ being number density, mass density, atomic mass unit and velocity averaged cross section, respectively[2].

[2] For convenience, the indices He and C denote ^{4}He and ^{12}C, respectively.

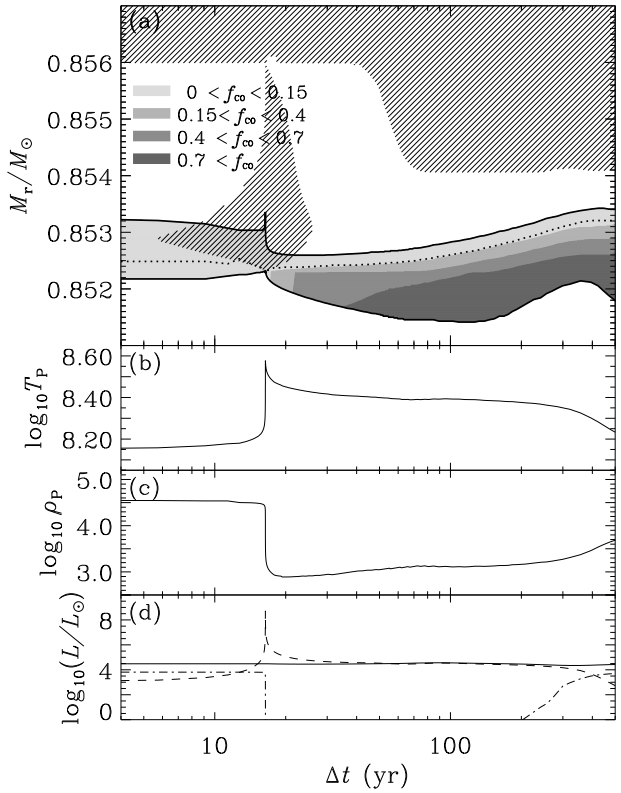

Figure 6. (a) Evolution of convective (hashed areas) and He-burning regions during a thermal pulse. The enclosed grey-scaled area marks the region where 90% of the He-burning energy is released. Each shade of grey indicates a different values of $f_{\rm CO}$ (Eq. (3)). The dotted line marks the location of the maximum in specific He-burning energy release rate. (b) Evolution of the temperature at the He-burning energy peak (dotted line in a). (c) The density at the same position. (d) The evolution of the total stellar luminosity (solid line), and of the specific H-burning (dash-dotted) and the He-burning energy release rate (dashed line).

The temperature-density stratification between $M_r/M_\odot = 0.8514$ and 0.8534 at $\Delta t = 16.4\,$yr (just before the peak in the He-energy release was reached) is represented by the dash-dotted line in Fig. 7. Since $f_\sigma^{\rm CO}$ barely exceeded 0.01, and the shell was still poor in ^{12}C, the number of ^{12}C+α reactions was very low, and thus the ISCZ was enriched mostly by ^{12}C. Even at $\Delta t = 20\,$yr, shortly after the helium flash, when the ISCZ had already withdrawn from the nuclear active region, most of the energy was still produced in regions where $f_\sigma^{\rm CO}$ was less than 0.1 (dashed line). In the subsequent evolution the He burning region started to contract, and the increasing density further

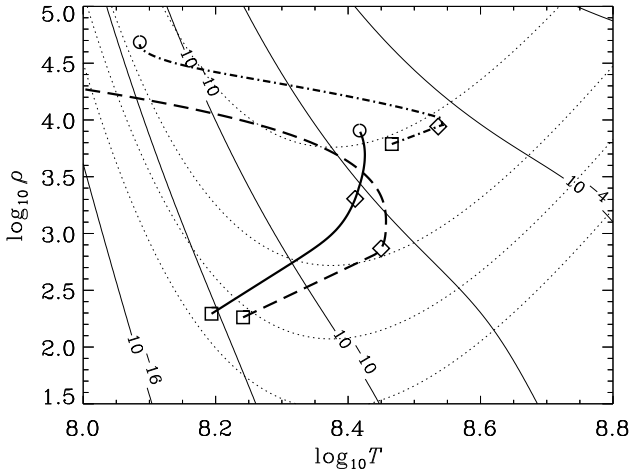

Figure 7. Relative and absolute efficiency of the ^{12}C+α and 3α reactions. The dotted lines mark the positions of $f_\sigma^{\rm CO} = 0.67$, 0.33, 0.1 and 0.01 (from bottom to top; Eq. (1)). The thin lines oriented dominantly vertically show equal values of $\sigma_n^{\rm C\alpha} + \sigma_n^{3\alpha}$ (in g s^{-1}mol^{-1}; Eq. (2)), separated in steps of 3 dex and indicating the overall efficiency of He-burning. The thick lines show the stratification of the shell with $0.8514 < M_r/M_\odot < 0.8534$ at $\Delta t = 16.4$ yr (dash-dotted), 20 yr (dashed) and 95 yr (solid line; cf. Fig. 6). Equal symbols mark equal mass shells, where □, ◇ and ○ are located at $M_r/M_\odot = 0.8534$, 0.8524 and 0.8514, respectively (cf. Fig. 6a).

disfavoured the ^{12}C+α rate (compare, e.g., the ◇'s on the dashed and solid line in Fig. 7).

However, with decreasing He abundance and thus increasing C abundance the 3α-rate

$$r_{3\alpha} = n_{\rm He}^3 \, \sigma_n^{3\alpha}$$

gradually weakened, while the opposite was true for the ^{12}C+α rate

$$r_{\rm C\alpha} = n_{\rm He} n_{\rm C} \, \sigma_n^{\rm C\alpha} \ ,$$

despite the shell became denser. Assuming, in a first approximation, that the burning shell consists only of α and ^{12}C, the minimum amount of He necessary to produce more C than O, can be determined (Fig. 8a) for different values of $f_\sigma^{\rm CO}$. Starting at $\Delta t = 20$ yr, along a Lagrangian shell in the He-burning region the reaction rate of ^{12}C+α became smaller (dotted line in Fig. 8a), and only a small amount of oxygen was produced (Fig. 8b). As soon as the helium abundance fell below a critical value (in this case $Y \approx 0.2$), however, $r_{\rm C\alpha}$ increased considerably, and the oxygen mass fraction eventually reached about 40 %.

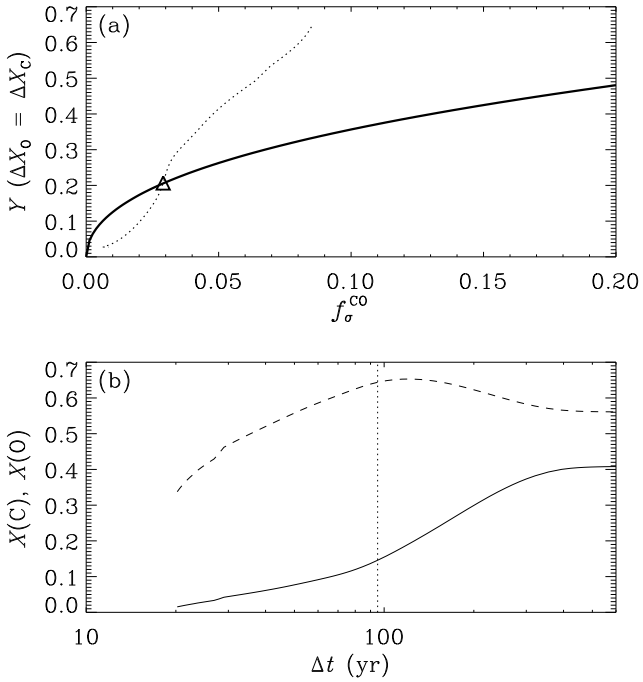

Figure 8. (a) Minimum helium mass fraction at which more C than O is produced for different values of the relative ^{12}C+α strength $f_\sigma^{\rm CO}$. Above the solid line the carbon production is favoured. The dotted line indicated the evolution of the shell $M_r/M_\odot = 0.8524$ from $\Delta t = 20$ yr onward (from top to bottom). The triangle marks the position where O production starts to become dominant over C production. (b) Evolution of the C (dashed) and O (solid line) mass fractions within the same shell as in (a). The dotted line indicates the moment denoted there by '△'.

But this material remains inside the star and is never brought to the surface, as no ISCZ occurred during the interpulse period, which could have bridged the region between H-burning and He-burning shells.

In Fig. 6a the actual contribution of ^{12}C$(\alpha,\gamma)^{16}$O to the He-burning reactions is shown, where

$$f_{\rm CO} = \frac{r_{\rm C\alpha}}{r_{3\alpha} + r_{\rm C\alpha}}. \qquad (3)$$

Clearly, the scenario outlined before is visible. During the He shell flash 3α reactions dominated over the whole burning region. Later, during quiescent He-burning, the outer shells in the burning regions still produced energy by the 3α-reaction. In deeper layers, which have been processed previously by 3α, and thus are C-rich, ^{12}C+α provided the main energy source.

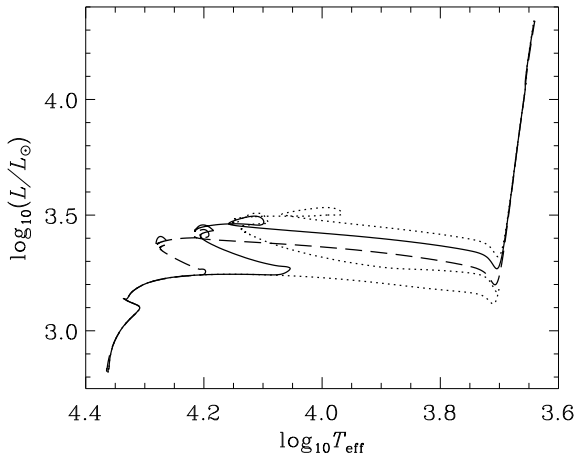

Figure 9. Evolution in the H-R diagram of models with different values of the 0_2^+ energy ($E_{\rm R}$) of ^{12}C for $\Delta E_{\rm R} = -105$ (dashed), 0 (solid), and +94 keV (dotted line). Only the evolution until the beginning of the TP AGB is displayed.

3.2.2. *Models with modified 3α-rate*

Modifying the 0_2^+ energy level of ^{12}C effectively alters the temperature at which He-burning reactions ignite. In Fig. 9 we show the evolutions of $5\,M_\odot$ stars with $\Delta E_{\rm R} = -105\,$keV, 0 keV and +94 keV. The different occurrences of He-ignition, i.e., when the stars are crossing the Hertzsprung gap, are clearly visible: the smaller the resonance energy the earlier the star stopped its evolution toward the red and became bluer again. When its core He-supply was consumed, it eventually settled on the AGB.

The overall evolution of the star in the H-R diagram is only mildly affected by a different 3α reaction. But at the altered He-burning temperature the result was a different ratio of the $^{12}\mathrm{C}(\alpha,\gamma)^{16}\mathrm{O}$-rate to the 3α-rate. Fig. 10 shows the strong sensitivity of the total C and O production of a $5\,M_\odot$ star to $E_{\rm R}$ (dash-dotted line). Changing the resonance energy by about $\pm 100\,$keV would yield a star which metal production essentially consists either completely of oxygen or of carbon (see also Table IV). This is similar to what has been found in Livio et al. (1989) and in Paper I.

Almost the same tendency of the C and O production could be observed, if just the phase during the TP AGB was considered, except that the underproduction of C was less pronounced. If only the abundances in the stellar wind or the stellar envelope were considered, which emerge through the 3$^{\rm rd}$ dredge-up process, a completely different picture ensues, in particular for the C production. The carbon production

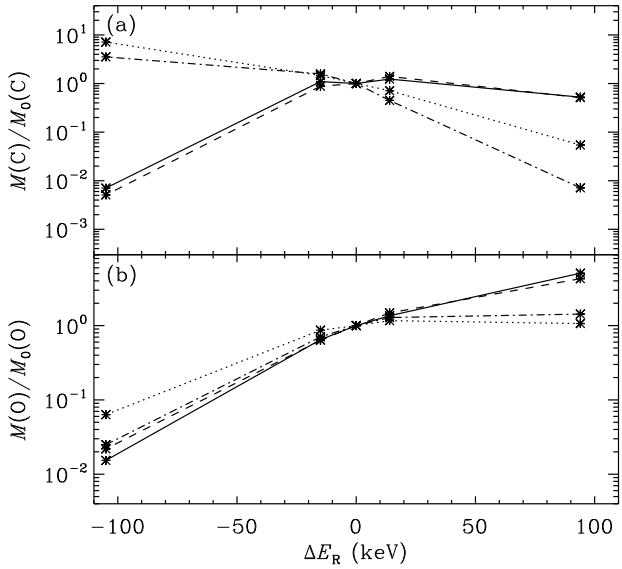

Figure 10. (a) Dependence of the C production on the 0_2^+ energy level relative to the standard case. The amount in the stellar wind is indicated by the dashed line, while the solid line represents the content in both envelope and wind. In addition, the complete amount of C created during the whole stellar lifetime (dash-dotted) and solely during the TP AGB (dotted line) are shown. The asterisks mark the actual models computed. (b) Like (a) but for oxygen.

was strongly suppressed when the resonance energy was lowered. But it was still about 40 % of the standard value, even for $\Delta E_{\rm R} = 100\,{\rm keV}$. This is nearly opposite of what was expected.

A closer look reveals that the underproduction of C and O for smaller values of $E_{\rm R}$ resulted because the He-shell flashes were weaker. During the interpulse period the temperature in the He-burning shell usually decreases while the density increases. As the He-burning temperature is reduced in this case, the He shell did not contract as much as before and thus less energy was needed to re-establish thermally stable conditions. The lower energy release in the shell flash led to a smaller ISCZ and after that also to a smaller overlap of the convective envelope with regions that had been part of the ISCZ. For the case of $E_{\rm R} = -100\,{\rm keV}$ no ISCZ developed and thus no 3$^{\rm rd}$ dredge-up occurred at all. The C and O abundances in the envelope were even smaller than their initial value. This is due to CN and ON-conversions in the CNO-cycle when the convective envelops deepens along the RGB and later on the AGB (Fig. 11a,b).

However, due to absence of a 3$^{\rm rd}$ dredge-up, the star maintained a metal-poor envelope and therefore the star remained relatively hot.

Table IV. C and O production of the $5\,M_\odot$ stars considering different stellar regions and/or phases.

	Summarized over whole star including the stellar wind			
	whole lifetime		during TP AGB	
$\frac{\Delta E_\mathrm{R}}{\mathrm{keV}}$	$\frac{M(\mathrm{C})}{M_\odot}$	$\frac{M(\mathrm{O})}{M_\odot}$	$\frac{M(\mathrm{C})}{M_\odot}$	$\frac{M(\mathrm{O})}{M_\odot}$
-105	1.08	0.015	0.25	0.0019
-15	0.48	0.42	0.051	0.026
0	0.31	0.59	0.036	0.030
$+14$	0.14	0.76	0.025	0.035
$+94$	0.0022	0.84	0.0019	0.032
	Integrated over whole stellar lifetime			
	wind		envelope + wind	
$\frac{\Delta E_\mathrm{R}}{\mathrm{keV}}$	$\frac{M(\mathrm{C})}{M_\odot}$	$\frac{M(\mathrm{O})}{M_\odot}$	$\frac{M(\mathrm{C})}{M_\odot}$	$\frac{M(\mathrm{O})}{M_\odot}$
-105	5.1×10^{-6}	7.5×10^{-6}	1.4×10^{-5}	8.3×10^{-6}
-15	0.00088	0.00022	0.0022	0.00035
0	0.0010	0.00034	0.0021	0.00054
$+14$	0.0014	0.00051	0.0025	0.00073
$+94$	0.00051	0.0015	0.0011	0.0027

This should inhibit the formation of dust-driven winds, and therefore our calculations assumed a much lower reduced mass-loss rate. The core mass grew considerably larger than in models with the standard 3α rate (cf. Fig. 11c). Although the $5\,M_\odot$ star remained below the Chandrasekhar mass, we expect that the limiting initial mass deciding whether stars become white dwarfs or evolve further into a supernovae would be shifted to a significantly lower value than in the standard case.

Since in supernova explosions parts of the He and the C/O core are ejected into the ISM as well, the overall ISM enrichment by C and O is larger per star. For the $5\,M_\odot$ star we found that the mass of oxygen produced for $E_\mathrm{R} = -105\,\mathrm{keV}$ during the TP AGB phase was $8.6 \times 10^{-4}\,M_\odot$, while in the standard case the wind and the envelope contained only $6.6 \times 10^{-4}\,M_\odot$ (Table IV). Hence considerable amounts of O could be created even in the case of a strongly reduced resonance energy.

In order to understand the case of increased resonance energy the dredge-up process has to be examined in detail. Fig. 12 outlines the evolution of a selected thermal pulse in a model with $\Delta E_\mathrm{R} = +94\,\mathrm{keV}$.

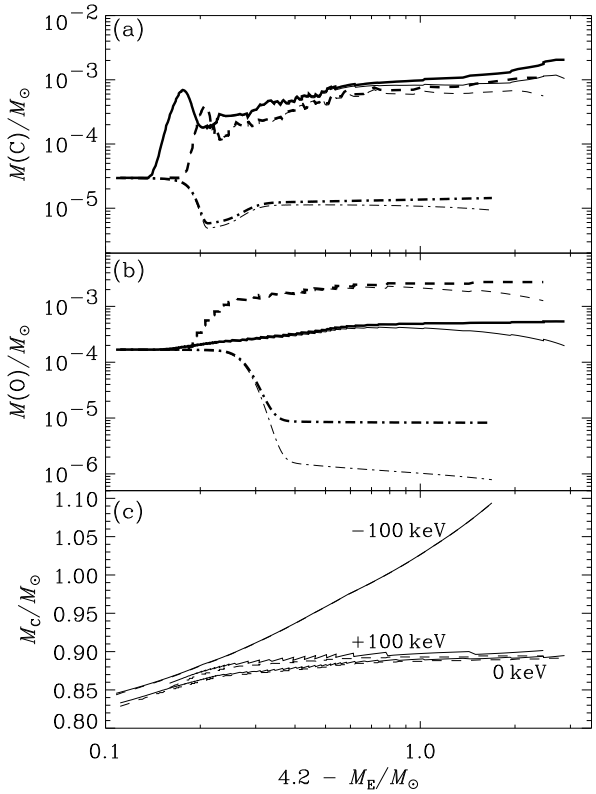

Figure 11. (a) Carbon production during the TP AGB as a function of decreasing envelope mass (M_E) for a 5 $M_\odot$ model with $\Delta E_\mathrm{R} = +100$ keV (solid), 0 keV (dashed) and -100 keV (dash-dotted line). The thick lines represent the total mass in wind and envelope, the thin lines solely the amount in the envelope. (b) Like (a) but for oxygen. (c) The evolution of the He- (solid) and C/O-core (dashed line) for the three cases.

Due to the slightly different lifetime of the star along the RGB and AGB the H-burning and He-burning shells were more widely separated than in the standard case (compare Figures 6a and 12a). Nevertheless, the energy produced in the He-shell flash was bigger, and, as in the standard case, the resulting convection zone comprised the entire H-free region between the two shells. The 3α-reaction remained the main source of energy at onset of the shell flash (see dash-dotted line in Fig. 13). Therefore carbon remained the main product. However, when the temperature and density decreased after the peak in the helium burning energy generation rate, L_He, the ^{12}C+α reaction contributed significantly and more oxygen was created than in the standard case (Fig. 12a).

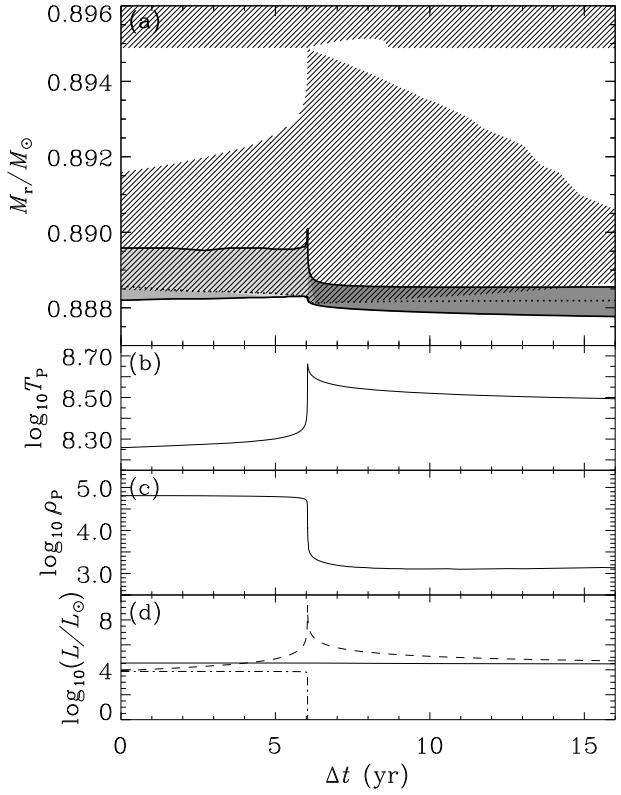

Figure 12. Same as Fig. 6, but the 0_2^+ resonance of ^{12}C has been increased by 94 keV.

Most of the energy was released around the time of the maximum in $L_{\rm He}$ and therefore most of the ^{12}C and ^{16}O nuclei were produced during a very short period ($\lesssim 1\,$yr). Since the 3α reactions were dominant in the early phases of the He-shell flash, a considerable amount of carbon could be produced. The receding ISCZ carries ^{12}C away from the active burning regions, preventing its destruction by $^{12}\mathrm{C}(\alpha,\gamma)^{16}\mathrm{O}$. The subsequent 3$^{\rm rd}$ dredge-up event enriched the envelope with C and O, so that the sum of final stellar envelope and wind still contain about 30–40 % of the carbon mass found in the star with unchanged resonance energy (Table IV).

In summary, the alternating phases of He-shell flashes and quiescent He-burning during the TP AGB produced a higher carbon to oxygen ratio than the earlier phases (Table IV). The composition of the material that enriched the envelope in the 3$^{\rm rd}$ dredge-up encountered nuclear burning during the very short period of the He-shell flash, which produced a higher C/O-ratio than was made in the inter-shell phase. To determine the C and O production of thermally pulsating stars and its

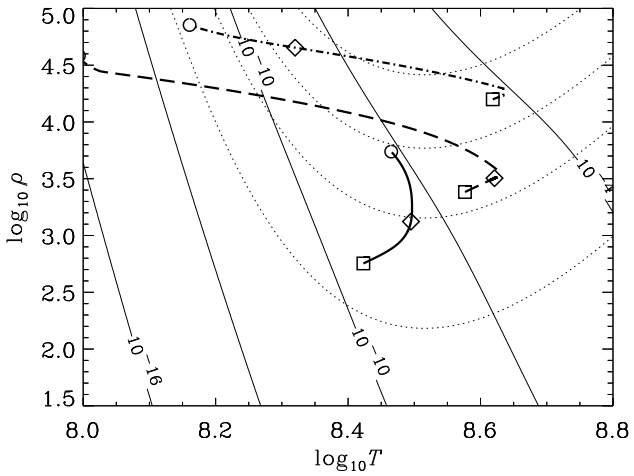

Figure 13. Same as Fig. 7, but the 0_2^+ resonance of ^{12}C has been increased by 100 keV. The dotted lines mark the positions of $f_\sigma^{\rm CO} = 0.95$, 0.67, 0.33 and 0.1 (from bottom to top; Eq. (1)). The thick lines show the stratification of the shell with $0.8877 < M_r/M_\odot < 0.8887$ at $\Delta t = 6$ yr (dash-dotted), 6.1 yr (dashed) and 15.5 *yr* (solid line; cf. Fig.6). Equal symbols mark equal mass shells, where □, ◇ and ○ are located at $M_r/M_\odot = 0.8877$, 0.8882 and 0.8887, respectively.

dependence on the 0_2^+ energy level in ^{12}C, it is hence crucial to follow accurately the He-shell flashes and the dredge-up events.

3.3. Low-mass stars

We followed the evolution of a $1.3\,M_\odot$ star from the zero-age main sequence (ZAMS) through the He flash until the final thermal pulses on the AGB for the same values of the resonance energy as for the $5\,M_\odot$ star. Though the lifetime of these stars is too long to influence the yields in the early universe, their C and/or O production might be important in anthropic reasonings for the fine-tuning of fundamental constants (see, e.g., Paper I).

Because of the smaller envelope mass of low-mass stars after the He-flash, the occurrence of a 3$^{\rm rd}$ dredge-up is much more sensitive to the amount of mass loss than for intermediate-mass stars. For instance, when using the same wind mass-loss description as for the intermediate-mass stars, our low-mass stellar models did not show a 3$^{\rm rd}$ dredge-up event. In this case, low-mass stars would not enrich the ISM with metals. However, observed C-enriched planetary nebulae with low-mass progenitors (see, e.g., Henry et al., 1996) show that the 3$^{\rm rd}$ is operating in these stars. Therefore, we have chosen a reduced stellar wind, i.e.,

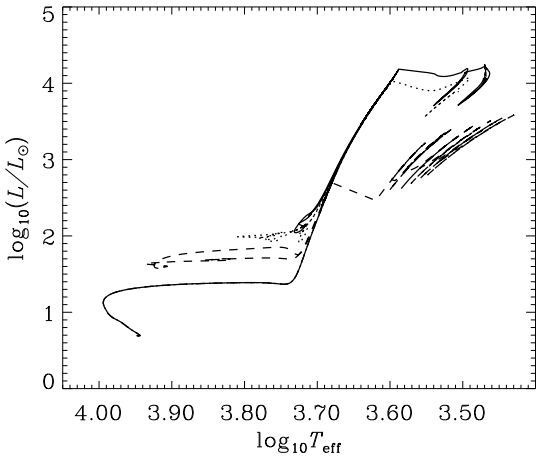

Figure 14. Evolution of $1.3\,M_\odot$ stars with $\Delta E_{\rm R} = -105\,$keV (dashed), 0 keV (dotted) and +94 keV (solid line) in the H-R diagram.

a pure Reimers wind with efficiency parameter $\eta = 0.25$. Using this description our $1.3\,M_\odot$ models showed a few thermal pulses which became sufficiently strong to lead to a 3$^{\rm rd}$ dredge-up.

3.3.1. *The standard case*

In Fig. 14 we show the evolution of a $1.3\,M_\odot$ star in the H-R diagram until the 3$^{\rm rd}$ dredge-up on the TP AGB. Note that we found a 2$^{\rm nd}$ dredge-up before the star started to pulsate thermally. This is different from the standard 2$^{\rm nd}$ dredge-up scenario of intermediate-mass stars: toward the end of the horizontal-branch evolution the H-burning shell became considerably weaker. When the star ascended the AGB, H burning re-ignited in a region comprising about $0.02\,M_\odot$, much more extended than the usual H-shell burning region, which is less than $0.001\,M_\odot$ during the late RGB or during the TP AGB phases. Although the H-burning shell becomes narrower rapidly, the established He profile remains above this shell, similar to the early RGB phase. During the subsequent evolution the convective envelope deepened and reached the outer tail of that He profile, increasing the mass fraction of He at the surface by about 0.002. The surface distribution of the CNO-elements remained unaltered, i.e., the same as after the 1$^{\rm st}$ dredge-up on the RGB.

The 2$^{\rm nd}$ dredge-up thus differs from that of intermediate-mass stars, where the convective envelope penetrated into the region of the H-burning shell, which was not active during the event. In low-mass stars the H-burning shell was active, but the envelope reached regions where

a He profile was left over from a previously wider H-burning region. In this sense, the mechanism of the 2$^{\rm nd}$ dredge-up in low-mass stars was similar to the 1$^{\rm st}$ dredge-up. This assessment is further supported by the unaltered surface CNO abundance distribution, which shows that the H-burning conditions in the areas engulfed by the growing convective envelope were similar to those at the sub-giant branch.

During the 4$^{\rm th}$ thermal pulse the He shell flashes became strong enough that the envelope convection zone penetrated into regions which were previously occupied by the ISCZ, i.e., a 3$^{\rm rd}$ dredge-up event occurred. Due to our mass-loss description only 2 further thermal pulses occurred before the envelope mass became less than about $10^{-3}\,M_{\odot}$, and the star evolved into the planetary-nebulae phase. The surface enrichment in C and O was not altered significantly by the subsequent 3$^{\rm rd}$ dredge-up events.

3.3.2. *Models with modified 3α-rate*

The change of the He-burning temperature in the models with modified 3α rate had various consequences for the evolution of low-mass stars. Due to the earlier onset of He-burning, the luminosity of the HB and of the AGB was reduced when lowering $E_{\rm R}$ (Fig. 14). Additionally, a stronger H-burning shell relative to the energy generation rate of the He-burning core leads to a more extended blue loop on the HB. Similarly, metal-poor stars show a more extended blue loop than their metal-rich counterparts because of their stronger H-burning shell. For higher values of $E_{\rm R}$ the opposite behaviour was observed.

The effect of the modified 3α-rate on the C and O production was as expected: the lower the resonance energy, the higher the C and the lower the O production (Fig. 15). Since the mechanism of the thermal pulses was the same as in the $5\,M_{\odot}$ star, a smaller sensitivity on $E_{\rm R}$ resulted also for the low-mass stars. In contrast to the $5\,M_{\odot}$ star, the $1.3\,M_{\odot}$ model with $\Delta E_{\rm R} = -105\,$keV did show the 3$^{\rm rd}$ dredge-up. The reason is the stronger degeneracy of the C/O core in the low-mass stars, leading to more energetic He-shell flashes. The extended TP AGB lifetime of the model with lowered resonance energy, and hence the higher number of pulses, compensated for the reduced O production per pulse. Overall, the O yield appears to be quite insensitive to moderate reductions of the resonance energy. However, the total amount of O produced in these stars was about an order of magnitude smaller than the C yield. Therefore, in the early universe, the contribution of these stars to O in the ISM is negligible. However, the much larger number of low-mass stars compared to intermediate-mass and massive stars, for a standard initial mass function, might still produce noticeable amounts of oxygen

Table V. Carbon and oxygen production of the $1.3\,M_\odot$ star for different stellar regions and/or phases.

	Summarized over whole star including the stellar wind			
	whole lifetime		during TP AGB	
$\frac{\Delta E_R}{\mathrm{keV}}$	$\frac{M(\mathrm{C})}{M_\odot}$	$\frac{M(\mathrm{O})}{M_\odot}$	$\frac{M(\mathrm{C})}{M_\odot}$	$\frac{M(\mathrm{O})}{M_\odot}$
−105	0.43	0.0030	0.088	0.00053
−15	0.30	0.25	0.028	0.012
0	0.21	0.38	0.036	0.029
+14	0.11	0.51	0.028	0.036
+94	0.0035	0.66	0.0031	0.073
	Integrated over whole stellar lifetime			
	wind		envelope + wind	
$\frac{\Delta E_R}{\mathrm{keV}}$	$\frac{M(\mathrm{C})}{M_\odot}$	$\frac{M(\mathrm{O})}{M_\odot}$	$\frac{M(\mathrm{C})}{M_\odot}$	$\frac{M(\mathrm{O})}{M_\odot}$
−105	0.013	4.8×10^{-5}	0.025	9.4×10^{-5}
−15	0.0011	2.6×10^{-5}	0.0050	9.6×10^{-5}
0	0.00072	3.1×10^{-5}	0.0035	0.00011
+14	0.0011	6.7×10^{-5}	0.0048	0.00022
+94	0.00033	0.00022	0.00093	0.00061

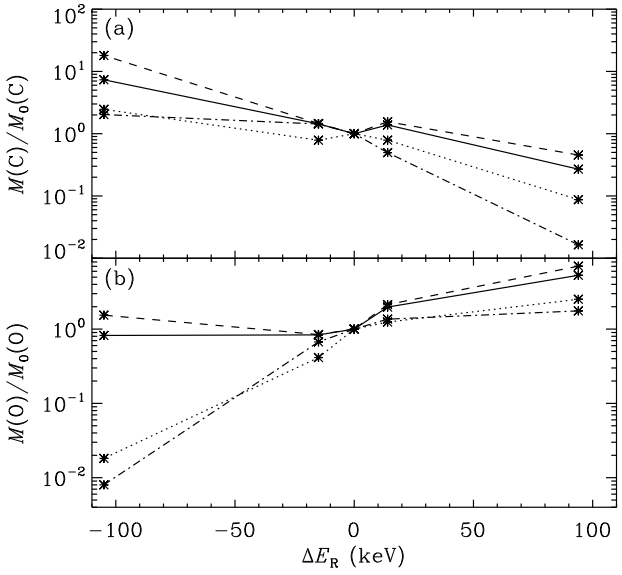

Figure 15. Dependence of the C (a) and O (b) production on the 0_2^+ energy level relative to the standard case. The line-styles correspond to Fig. 10.

after a few billion years, i.e., they could considerably enrich the ISM at a later time.

4. Conclusions

We provide an improved determination of the dependence of the C and O production on the 0_2^+ resonance energy in low-mass, intermediate-mass, and massive stars. Our results show that the C and O production in massive stars depends on the initial stellar mass and, overall, is somewhat smaller than estimated in Paper I. Possible reasons are the different treatment of semiconvection and the different $^{12}C(\alpha,\gamma)^{16}O$ reaction rate.

Massive stars are the primary source of nucleosynthesis in the early universe, and their yields determine the C and O content of very metal-poor stars.

If the early universe had a different 3α rate caused, e.g., by a varying fine-structure constant, then in particular the C/O ratio would be different than in standard galacto-chemical models. Though current standard models are well able to reproduce the observed abundances, an uncertainty of about 50 % in the theoretical yields at very low metallicities remains (see, e.g., Liang et al., 2001, for an overview). In Table VI we provide the relative changes of the final C/O yield of our massive star models for $\Delta E_{\rm R} = \pm 100\,{\rm keV}$ compared to the standard case. A coarse upper limit on the possible variations of $\Delta E_{\rm R}$ can be obtained by not allowing the change in the C/O ratio in those stars to become larger than the error in the standard yields of about 50 %. By linear interpolation of the results in Table VI $\Delta E_{\rm R}$ is constrained to about $-5\,{\rm keV}$ to $+50\,{\rm keV}$. Hence, based on our results, any possible change in a fundamental constant that causes a shift in $E_{\rm R}$ larger than this would be inconsistent with observations. A more accurate determination of the allowed values of $\Delta E_{\rm R}$ would require models with different $\Delta E_{\rm R}$ and different masses. Their yields would have to be integrated over an initial mass function to obtain population average values.

Intermediate-mass stars do not provide more stringent constraints. We found that the sensitivity of their C and O production is considerably smaller than determined in Paper I. There the C and O yields of low- and intermediate-mass stars were obtained by determining the abundances within the He-burning shell *after* the 3$^{\rm rd}$ thermal pulse. Clearly, by that method the carbon production for $\Delta E_{\rm R} > 0$ was strongly underestimated, because significant amounts of C are produced during the He-shell flash. Only during this short period an ISCZ exists which brings C-rich and O-rich material close to the H-rich

Table VI. Relative change in the yield ratio $M_{\rm SN}({\rm C})/M_{\rm SN}({\rm O})$ ('C/O-ratio') for massive stars (Table I) compared to the standard case ($\Delta E_{\rm R} = 0$).

$\frac{\Delta E_{\rm R}}{\rm keV}$	$15\,M_\odot$	$25\,M_\odot$
−100	33	28
0	1	1
+100	0.34	0.11

convective envelope. In the ensuing evolution, the base of convective envelope deepened and thereby enriched the surface by material processed by He burning.

For lower resonance energies the situation was even more involved. The smaller extent of the ISCZ strongly reduced the dredge-up, causing a significant reduction of the C *and* O enrichment of the envelope. However, the reduced surface enrichment caused a lower mass-loss rate and led to more massive C/O core. This could cause a reduction of the limiting initial mass for core collapse supernovae. More C and O rich material would be ejected into the ISM than by stellar winds of TP AGB stars. Thus even for $\Delta E_{\rm R} < 0$ the absolute oxygen mass in the ISM might be significant, although the C/O ratio would be large. A more accurate determination would require population-synthesis computations. This is beyond the aim of this paper, however.

In low-mass stars the 3$^{\rm rd}$ dredge-up was never suppressed by the variations of $\Delta E_{\rm R}$ considered. The higher number of thermal pulses for $\Delta E_{\rm R} < 0$ almost compensated for the reduced O production per pulse. However, the oxygen yields of low-mass stars are very small, and they would not contribute noticeably to the O enrichment of the ISM for many billion years.

Summarizing, when the evolution of the stars as a whole was followed for their entire life, in particular the low- and intermediate-mass stars show fine tuning of carbon and oxygen yields that is more complicated and far less spectacular than found in Paper I. Therefore, the anthropic significance of the 3α rate might be of considerably less.

Acknowledgements

This work was promoted by the John Templeton Foundation (938-COS153). H.S. has been supported by a Marie Curie Fellowship of the European Community programme 'Human Potential' under contract

number HPMF-CT-2000-00951. A.H. has been supported by the Departement of Energy under contract W-7405-ENG-36, by the Department of Energy under grant B341495 to the Center for Astrophysical Thermonuclear Flashes at the University of Chicago, and a Fermi Fellowship at the University of Chicago. T.R. acknowledges a PROFIL professorship from the Swiss National Science foundation (grant 2024-067428.01) and the support from the Swiss NSF (2000-061031.02). A.C. was supported by OTKA-T037548/FKFP-0147-2001.

References

Adelberger, E. G., S. M. Austin, J. N. Bahcall, A. B. Balantekin, G. Bogaert, et al.: 1998. *Rev. Mod. Phys.* **70**, 1265.

Alexander, D. R. and J. W. Fergusson: 1994. *ApJ* **437**, 879.

Böhm-Vitense, E.: 1958. *Z. Astrophys.* **46**, 108.

Buchmann, L.: 1996. *ApJ* **468**, 127.

Calmet, X. and H. Fritsch: 2002. *Eur. Phys. J. C* **24**, 639.

Cassisi, S., M. Salaris, and A. W. Irwin: 2003a. *ApJ* **588**, 862.

Cassisi, S., H. Schlattl, M. Salaris, and A. Weiss: 2003b. *ApJ* **582**, L43.

Caughlan, G. R., W. A. Fowler, M. J. Harris, and B. A. Zimmerman: 1985. *Atomic Data Nuc. Data Tables* **32**, 197.

Chacko, Z., C. Grojean, and M. Perelstein: 2002, 'Fine Structure Constant Variation from a Late Phase Transition'. Saclay T02/038, hep-ph/0204142.

Cook, C. W., W. A. Fowler, C. C. Lauritsen, and T. Lauritsen: 1957. *Phys. Rev.* **107**, 508.

Dent, T. and M. Fairbairn: 2003. *Nucl. Phys. B* **653**, 256.

Faulkner, D. J.: 1970. *ApJ* **162**, 513.

Finzi, A. and R. A. Wolf: 1971. *A&A* **11**, 418.

Fiorentini, G. and B. Ricci: 2002. In: *Proc. of ESO-CERN-ESA Symposium on Astronomy, Cosmology and Fundamental Physics, Garching, Germany, 4–7 March 2002*.

Firestone, R. B., V. S. Shirley, C. M. Baglin, S. Y. F. Chu, and J. Zipkin: 1996, *Table of Isotopes*. New York: John Wiley & Sons, Inc., eighth edition.

Heger, A., N. Langer, and S. E. Woosley: 2000. *ApJ* **528**, 368.

Heger, A., S. E. Woosley, T. Rauscher, R. D. Hoffman, and M. M. Boyes: 2002. *New Astron. Rev.* **46**, 463.

Henry, R. B. C., K. B. Kwitter, and J. W. Howard: 1996. *ApJ* **458**, 215.

Hoyle, F.: 1954. *ApJS* **1**, 121.

Hoyle, F., D. N. F. Dunbar, W. A. Wenzel, and W. Whaling: 1953. *Phys. Rev.* **92**, 1095.

Iglesias, C. A. and F. J. Rogers: 1996. *ApJ* **464**, 943.

Janka, H.-T., R. Buras, K. Kifonidis, M. Rampp, and T. Plewa: 2002. In: W. Hillebrandt and B. Leibundgut (eds.): *From Twilight to Highlight: The Physics of Supernovae*. Berlin: Springer Verlag, in press

Kippenhahn, R. and A. Weigert: 1990, *Stellar Structure and Evolution*. Berlin, Heidelberg: Springer-Verlag.

Kunz, R., M. Fey, M. Jaeger, A. Mayer, J. W. Hammer, et al.: 2002. *ApJ* **567**, 643.

Kunz, R., M. Jaeger, A. Mayer, J. W. Hammer, G. Staudt, et al.: 2001. *Phys. Rev. Lett.* **86**, 3244.
Langacker, P., G. Segrè, and M. J. Strassler: 2002. *Phys. Lett. B* **528**, 121.
Langanke, K., M. Wiescher, and F.-K. Thielemann: 1986. *Z. Phys. A* **324**, 147.
Langer, N., M. El Eid, and K. J. Fricke: 1985. *A&A* **145**, 179.
Liang, Y. C., G. Zhao, and J. R. Shi: 2001. *A&A* **374**, 936.
Limongi, M., O. Straniero, and A. Chieffi: 2000. *ApJS* **129**, 625.
Livio, M., D. Hollowell, A. Weiss, and J. W. Truran: 1989. *Nature* **340**, 281.
Marigo, P., A. Bressan, and C. Chiosi: 1996. *A&A* **313**, 545.
Murphy, M. T., J. K. Webb, V. V. Flambaum, M. J. Drinkwater, F. Combes, and T. Wiklind: 2001. *MNRAS* **327**, 1244.
Nieuwenhuijzen, H. and C. de Jager: 1990. *A&A* **231**, 134.
Oberhummer, H., A. Csótó, M. Fairbairn, H. Schlattl, and M. M. Sharma: 2003. *Nucl. Phys. A* **719**, 283c.
Oberhummer, H., A. Csótó, and H. Schlattl: 2000. *Sci* **289**, 88 (Paper I).
Oberhummer, H., A. Csótó, and H. Schlattl: 2001. *Nucl. Phys. A* **689**, 269c.
Rauscher, T., A. Heger, R. D. Hoffman, and S. E. Woosley: 2002. *ApJ* **576**, 323.
Reimers, D.: 1975. *Mem. Soc. Roy. Sci. Liège* **8**, 369.
Rogers, F. J., F. J. Swenson, and C. A. Iglesias: 1996. *ApJ* **456**, 902.
Schlattl, H.: 1999. Ph.D. thesis, Technical University Munich.
Schlattl, H.: 2002. *A&A* **395**, 85.
Schlattl, H., S. Cassisi, M. Salaris, and A. Weiss: 2001. *ApJ* **559**, 1082.
Vassiliadis, E. and P. R. Wood: 1993. *ApJ* **413**, 641.
Wagenhuber, J. and A. Weiss: 1994. *A&A* **286**, 121.
Weaver, T. A. and S. E. Woosley: 1993. *Phys. Rept.* **227**, 65.
Weaver, T. A., G. B. Zimmermann, and S. E. Woosley: 1978. *ApJ* **225**, 1021.
Weiss, A. and H. Schlattl: 2000. *A&AS* **144**, 487.
Wood, P. R. and D. J. Faulkner: 1986. *ApJ* **307**, 659.
Woosley, S. E., A. Heger, T. Rauscher, and R. D. Hoffman: 2003. *Nucl. Phys. A* **718**, 3c.
Woosley, S. E., A. Heger, and T. A. Weaver: 2002. *Rev. Mod. Phys.* **74**, 1015.
Woosley, S. E. and T. A. Weaver: 1995. *ApJS* **101**, 181.